Research Paper

miR-30c-1 encourages human corneal endothelial cells to regenerate through ameliorating senescence

Younghwan Bae[1,*], Jin Sun Hwang[1,*], Young Joo Shin[1]

[1]Department of Ophthalmology, Hallym University Medical Center, Hallym University College of Medicine, Seoul, Republic of Korea
[*]Equal contribution

Correspondence to: Young Joo Shin; **email:** schinn@hallym.or.kr
Keywords: miR-30c-1, human corneal endothelial cells, senescence, proliferation, TGF-β
Received: May 11, 2020 **Accepted:** February 16, 2021 **Published:** March 19, 2021

ABSTRACT

In the present study, we studied the role of microRNA-30c-1 (miR-30c-1) on transforming growth factor beta1 (TGF-β1)-induced senescence of hCECs. hCECs were transfected by miR-30c-1 and treated with TGF-β1 to assess the inhibitory effect of miR-30c-1 on TGF-β1-induced senescence. Cell viability and proliferation rate in miR-30c-1-transfected cells was elevated compared with control. Cell cycle analysis revealed that cell abundance in S phase was elevated in miR-30c-1-treated cells compared with control. TGF-β1 increased the senescence of hCECs; however, this was ameliorated by miR-30c-1. TGF-β1 increased the size of hCECs, the ratio of senescence-associated beta-galactosidase-stained cells, secretion of senescence-associated secretory phenotype factors, the oxidative stress, and arrested the cell cycle, all of which were ameliorated by miR-30c-1 treatment. miR-30c-1 also suppressed a TGF-β1-induced depolarization of mitochondrial membrane potential and a TGF-β1 stimulated increase in levels of cleaved poly (ADP-ribose) polymerase (PARP), cleaved caspase 3, and microtubule-associated proteins 1A/1B light chain 3B II. In conclusion, miR-30c-1 promoted the proliferation of hCECs through ameliorating the TGF- β1-induced senescence of hCECs and reducing cell death of hCECs. Thus, miR-30c-1 may be a therapeutic target for hCECs regeneration.

INTRODUCTION

Human corneal endothelial cells (hCECs) are characterized as playing a pivotal role in making the cornea transparent and as not regenerating *in vivo* [1]. In response to injury, hCECs undergo compensatory cellular hypertrophy, which is characterized by increased size and migration of adjacent cells [2, 3]. If the enlarged hCECs no longer compensate the function [2], it results in the bullous, and painful corneal edema [4]. Proliferation of hCECs is blocked *in vivo*, and therefore, there is no alternative to transplantation in hCEC-related disease. Understanding the mechanism that blocks the proliferation of hCECs and temporarily resolving this may be valuable for regenerative treatment of hCEC disease. Cellular senescence is accompanied by a loss of proliferation capacity, cell cycle cessation, and cellular hypertrophy. These changes are similar to changes in hCEC seen *in vivo* during the wound healing process. Thus, inhibition of senescence may be a key mechanism for regeneration of hCECs.

MicroRNA (miRNA) is a short non-coding RNA molecule that is involved in gene expression [5]. It is single-stranded and composed of ~20–25 nucleotides in length [5]. The RNase III enzyme Dicer cleaves the pre-miRNA hairpin to miRNA-5p and miRNA-3p [6]. The 5p strand is located in the forward, and the 3p strand in the reverse [6]. The key function of miRNAs degrades or inhibits messenger RNAs (mRNAs) translation through binding to the complementary mRNAs. miR-30c has been found in murine corneal endothelial cells and is decreased in expression in Fuchs' corneal

endothelial dystrophy (FECD) [7]. The miR-30c family includes miR-30c-1 and miR-30c-2, and their functions may be differ due to sequence differences of miRNA-3p. The role of miR-30c-1 has been controversial, although miR-30c-1 has been suggested to promotes cell cycle progression [8, 9]. while regulation of miR-30c-1 may induce regeneration of hCECs.

Thus, in the present study, we investigated the regulatory role of miR-30c-1 on hCEC regeneration and on TGF-β1-induced senescence of hCECs.

RESULTS

miR-30c-1 promotes the proliferation of hCECs

Cell viability and proliferation

miR-30c level was elevated in miR-30c-1-treated cells compared with miR-control ($p < 0.001$, Figure 1A). hCEC size decreased with miR-30c-1-treatment compared with control ($p < 0.001$, Figure 1B). Cell viability and proliferation rate were elevated in miR-30c-1-treated cells compared with miR-control ($p < 0.001$ and 0.040; Figure 1C–1D). The cellular abundance in S-phase of cell cycle was higher in miR-30c-1-treated cells compared with miR-control ($p = 0.001$; Figure 1E).

RNA sequencing

Normalized read counts and fold changes are shown in Figure 2A and Table 1. Relative expressions of cell proliferation-associated genes were elevated and relative expressions of inhibitor genes were reduced in miR-30c-1-treated cells compared with miR-control ($p < 0.05$ for all, Figure 2B, Table 1). Interferon (IFN)-associated genes (Figure 2C), TGF-β-associated genes (Figure 2D), caspases genes (Figure 2E) and autophagy-associated genes (Figure 2F) were decreased in miR-30c-1-treated cells compared with miR-control ($p < 0.05$ for all).

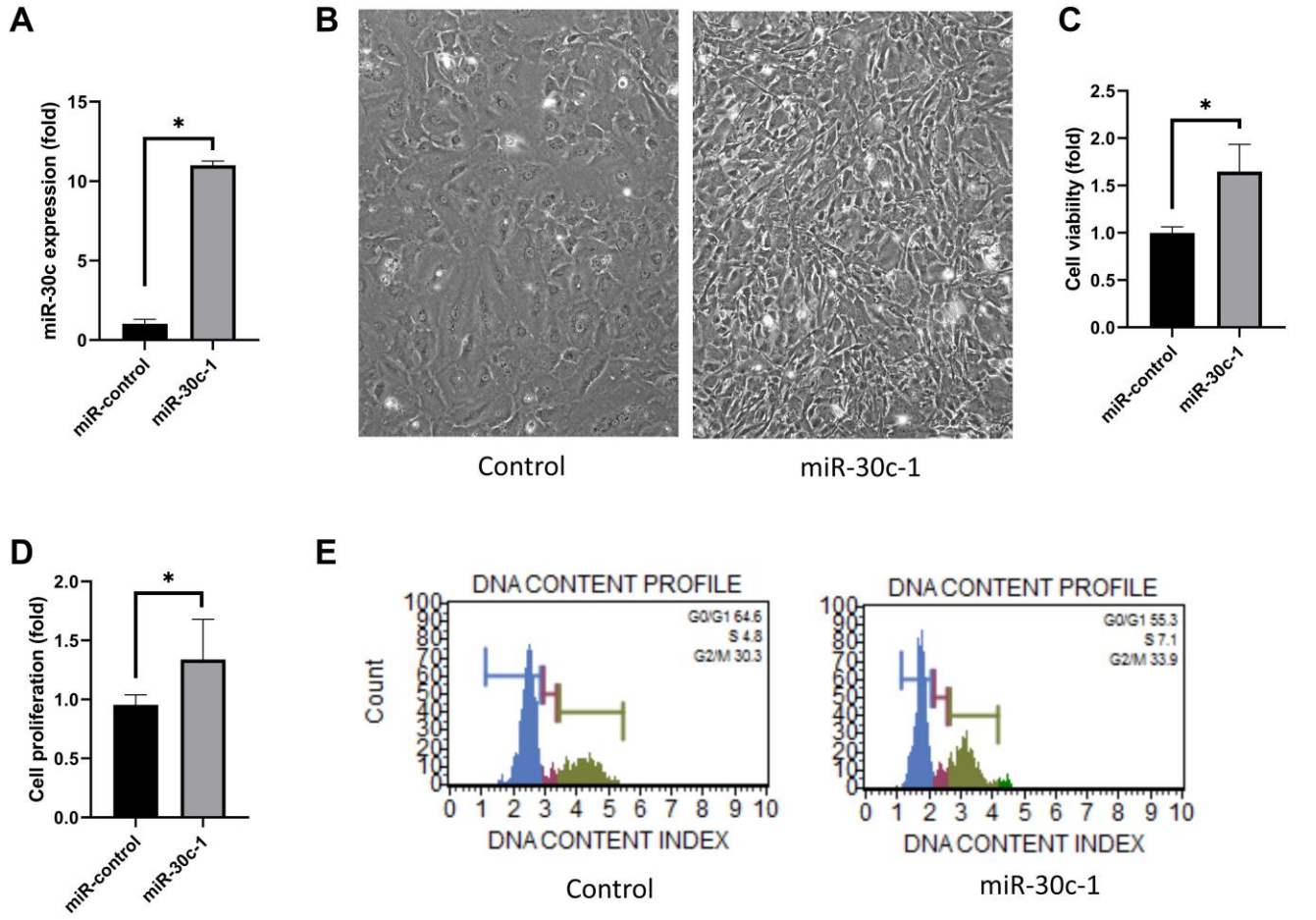

Figure 1. Cell proliferation induced by miR-30c-1. (**A**) miR-30c level was elevated in miR-30c-1-treated cells compared with miR-control. (**B**) Representative images of cell shape in control and in miR-30c-1-treated cells. (**C**) Cell viability in control and in miR-30c-1-treated cells measured by CCK-8 assay. (**D**) Cell proliferation in control and in miR-30c-1-treated cells measured by BrdU proliferation assay. (**E**) Cell cycle analysis showing that miR-30c-1 elevated the percentage of cells with S-phase. *statistically significant.

Table 1. Specific fold change (FC) values in differentially expressed genes.

Gene symbol	Fold Change (miR-30c-1/miR-control)	Log2(FC)	*p*-value
IFIT2	0.0099863	–6.6458342	0.0001552
BST2	0.0174225	–5.8429032	0.0002403
IFI27	0.0365895	–4.7724258	0.0013726
OAS1	0.0395716	–4.6593894	5.41E-05
ALK	0.0468338	–4.4163052	0.0004983
IFNB1	0.0488735	–4.3548048	0.0004183
SLC8A2	0.0612903	–4.0281969	0.0025017
HLA-F	0.0840182	–3.5731542	0.000448
IFI44	0.0879615	–3.5069838	1.523E-05
STAT1	0.0918394	–3.4447428	3.58E-05
PARP9	0.1054564	–3.245281	2.907E-05
IFI35	0.1171023	–3.0941583	7.448E-06
IFNB1	0.1278718	–2.9672301	0.0001676
TNFSF10	0.1417435	–2.8186455	0.0014769
IFNA1	0.2279793	–2.1330254	0.0397558
CASP1	0.260129	–1.9427008	0.0065726
STAT2	0.3039028	–1.7183184	1.162E-05
IFI16	0.3461232	–1.5306425	3.402E-05
CD7	0.3552655	–1.4930304	0.0017694
CASP3	0.4122607	–1.2783713	0.0001307
CD34	0.4330144	–1.2075132	0.0011659
CASP10	0.5226783	–0.936005	6.75E-06
TGIF2	0.5345843	–0.9035108	7.346E-05
NOTCH1	0.5389247	–0.8918443	0.0094308
IFNGR2	0.5688129	–0.8139739	5.281E-05
CASP4	0.6067611	–0.7207996	0.0005647
CASP7	0.6100666	–0.7129612	0.0002713
CIP2A	0.620878	–0.6876182	0.0123176
ATG12	0.6714314	–0.574688	0.000519
ACP2	0.6991534	–0.516319	0.0004251
WNT11	0.7069583	–0.5003031	0.0078715
ATG5	0.7276916	–0.4586009	0.0007922
SMAD1	0.737237	–0.4397997	0.0010524
CASP8	0.7388248	–0.4366958	0.0077211
CDKN2A	0.7620468	–0.3920485	0.0317108
WNT5B	0.7692308	–0.3785116	0.000321
WNT5A	0.7734093	–0.370696	0.0008211
CDKN2B	0.7921014	–0.336243	0.0068403
IGF2R	0.8032468	–0.3160849	0.0092538
SMAD3	0.8175286	–0.2906589	4.86E-05
NOTCH2	0.8281981	–0.2719522	0.018508
BECN1	0.8411694	–0.2495317	0.006372
CASP9	0.8435622	–0.2454336	0.0077383
PDGFA	0.8585895	–0.2199595	0.0460734
MAPK1	0.893772	–0.1620212	0.0311704

COL8A1	1.0841073	0.1165076	0.0492557
SIRT1	1.1383886	0.1869932	0.0403678
MFF	1.200156	0.2632219	0.0073113
CCNG1	1.2523403	0.3246267	0.0001706
COL8A2	1.2644785	0.3385425	0.0206073
CCNG2	1.2872408	0.364282	0.0006619
CDC25B	1.4089818	0.494653	0.0064732
CCNA2	1.4467974	0.5328629	0.0382018
CCND2	1.4973629	0.5824239	0.0018972
CEMIP	1.502362	0.5872325	0.0174476
CDK6	1.5484987	0.6308702	0.0041804
COL4A4	1.5797686	0.6597133	0.0199125
SOD2	1.7181873	0.7808874	0.0058297
SLC4A11	1.7909408	0.8407176	0.0041401
SLC25A15	1.8435085	0.8824541	2.931E-05
CEMIP2	1.8807528	0.9113102	0.000163
MTFP1	1.8954822	0.9225649	0.0119586
FOXO3	1.9359241	0.9530224	0.0002565
COL17A1	2.0654762	1.0464744	0.0044258
SOX7	2.1077586	1.0757097	0.0342846
AQP7	2.2103896	1.1443007	0.0256781
HTR2A	2.3896723	1.2568128	0.0018409
GPR20	4.5950413	2.2000778	0.0123495
GPR158	8.34	3.0600474	0.0244592
COL5A3	16.64	4.0565835	0.0360859

Mitochondrial functions

DCF fluorescence intensity decreased in miR-30c-1-treated cells compared with miR-control ($p < 0.001$; Figure 3A–3B). Intracellular oxidative stress level measured by Muse analyzer decreased in miR-30c-1-treated cells compared with miR-control ($p = 0.006$; Figure 3C–3D). The mitochondrial membrane potential increased in miR-30c-1-treated cells compared with miR-control ($p < 0.001$; Figure 3E–3F).

miR-30c-1 ameliorates TGF-β1-induced senescence of hCECs

Cell cycle analysis was conducted using quantitation of DNA content (Figure 4A). Cell cycle analysis presented that the cellular abundance in G0/G1 phase was elevated following TGF-β1 treatment, but it was not elevated with miR-30c-1 treatment ($p = 0.010$; Figure 4B). The cellular abundance in S-phase and in G2/M-phase was reduced with TGF-β1 treatment compared with miR-30c-1 treatment ($p = 0.001$; Figure 4C–4D). TGF-β1 stimulation also significantly increased cell size ($p = 0.017$) compared with miR-30c-1 treatment ($p = 0.001$; Figure 4E–4F). TGF-β1 caused an elevation in yes-associated protein (YAP) levels compared with miR-30c-1 treatment ($p = 0.041$ and $p = 0.033$, respectively; Figure 4G–4H). miR-30c-1 levels were reduced in treatment with TGF-β1 ($p = 0.041$, Figure 4I).

The ratio of SA-β-gal-stained cells was elevated with TGF-β1 treatment ($p = 0.008$), which did not occur when miR-30c-1 was present ($p = 0.007$; Figure 5A–5B). Intracellular oxidative stress was increased following TGF-β1 treatment ($p = 0.035$) but was ameliorated by miR-30c-1 ($p = 0.002$; Figure 5C). Additionally, TGF-β1 treatment also increased the levels of p-p38 and p63 ($p = 0.013$ and $p = 0.019$, respectively), but these did not increase when miR-30c-1 was present ($p = 0.047$ and $p = 0.043$, respectively; Figure 5D–5G).

Evaluation of SASPs in conditioned medium demonstrated that the levels of IL-6, TNF-α, and MIF increased after TGF-β1 treatment ($p = 0.030$, $p < 0.001$, and $p < 0.010$, respectively), which did not occur following miR-30c-1 treatment ($p = 0.005$, $p < 0.001$, and $p = 0.021$, respectively; Figure 6A–6C). The percentage of NF-κB located in the nucleus was

elevated by TGF-β1 but was ameliorated by miR-30c-1 (p = 0.001 and p = 0.002, respectively; Figure 6D–6E). TGF-β1 also elevated the levels of pERK1/2 and SMAD2/3 (p = 0.003 and p = 0.012, respectively) but not when miR-30c-1 was present (p = 0.048 and p = 0.013; Figure 6F–6I). Additionally, IGF-1 and PDGF-BB levels were also increased with TGF-β1 treatment (p = 0.001 and p = 0.032, respectively) but not in the presence of miR-30c-1 (p = 0.183 and 0.044; Figure 6J–6K).

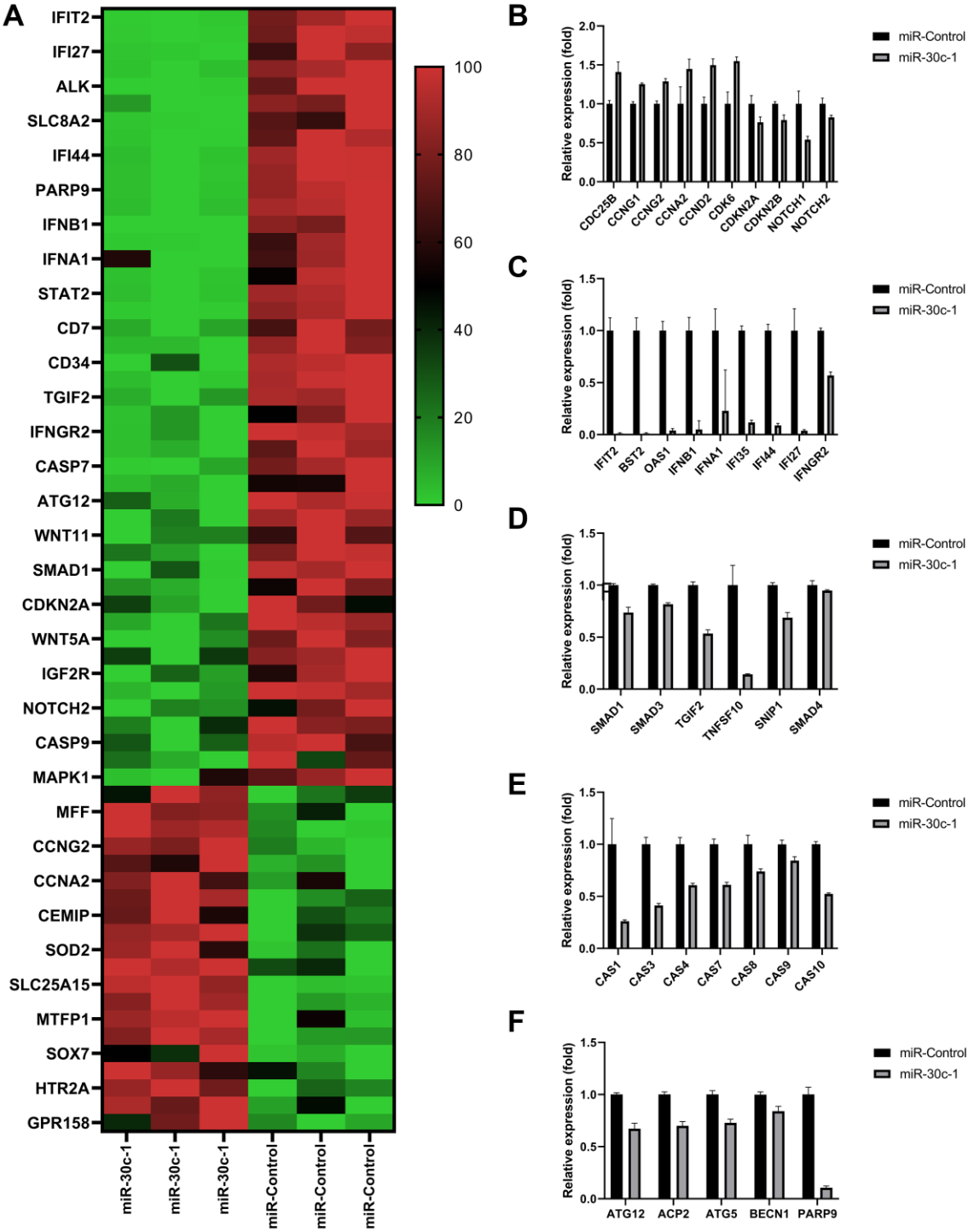

Figure 2. Results of RNA-sequencing data. (**A**) Heat map of the relative expression of differentially expressed genes. Comparison of relative expressions of proliferation-associated genes (**B**), interferon (IFN)-associated genes (**C**), transforming growth factor (TGF; (**D**)) caspases (**E**) and autophagy (**F**) between miR-control group and miR-30c-1 group. *statistically significant.

miR-30c-1 ameliorates TGF-β1-induced cell death of hCECs

TGF-β1 treatment promoted the depolarization of mitochondrial membrane potential (p = 0.014) but this effect was eliminated with miR-30c-1 treatment (p = 0.003, Figure 7A). In addition, TGF-β1 elevated the levels of cleaved caspase 9, cleaved PARP, and cleaved caspase 3 (p = 0.034, p = 0.012, and p = 0.049, respectively), but the presence of miR-30c-1 ameliorated this effect (p = 0.047, p = 0.019, and p = 0.011, respectively; Figure 7B–7F).

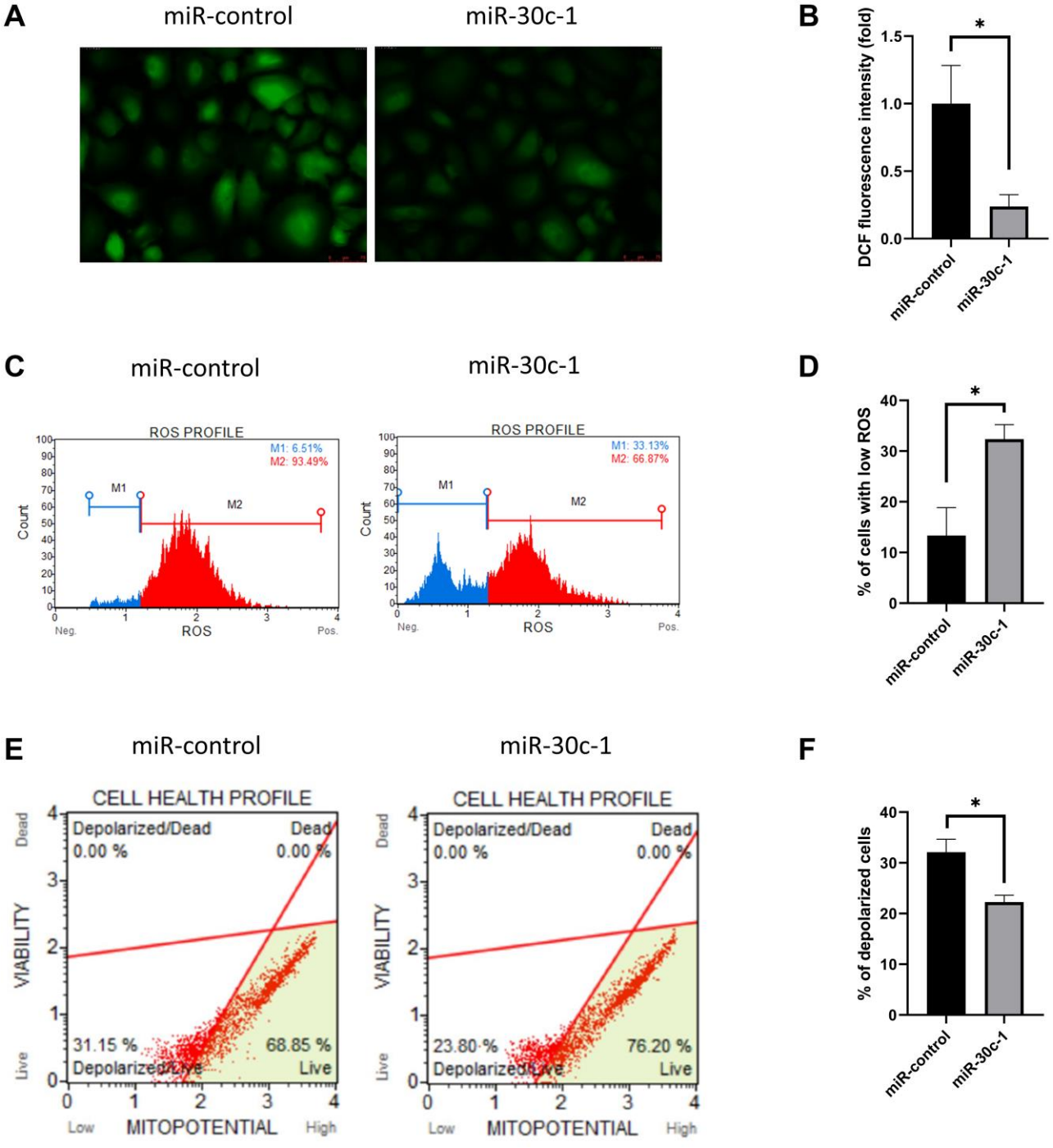

Figure 3. Oxidative stress level and mitochondrial membrane potential changed by miR-30c-1. (**A**) Representative images of dichlorofluorescin diacetate staining in control and miR-30c-1-treated cells. (**B**) DCF fluorescence intensity in control and miR-30c-1-treated cells. (**C**–**D**) Fluorescence intensity of MitoSOX probe was measured by Muse cell analyzer. (**E**–**F**) Mitochondrial membrane potential was measured using Muse® MitoPotential kit.

Lysosomes (green stain) became enlarged and prominent following TGF-β1 treatment, while this effect was removed with miR-30c-1 treatment (Figure 8A). The level of LC3II also increased after TGF-β1 treatment ($p < 0.001$) but not when miR-30c-1 was present ($p < 0.001$; Figure 8B–8C).

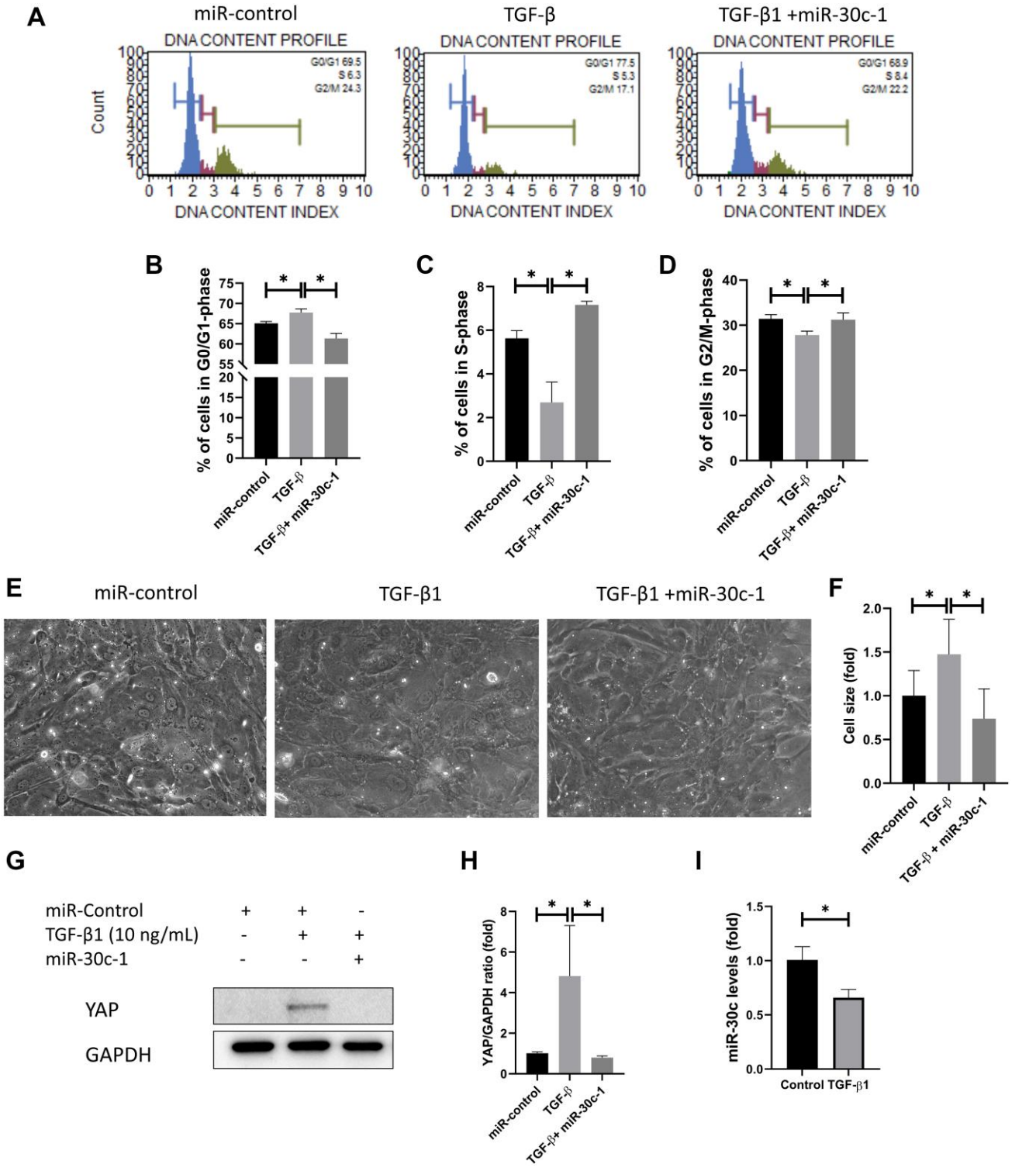

Figure 4. miR-30c-1 ameliorates TGF-β1-induced cell cycle arrest. (**A**) Cell cycle analysis was analyzed using DNA content. (**B**) The percentage of cells in S-phase. (**C**) The percentage of cells in G0/G1 phase. (**D**) The percentage of cells in G2/M phase. (**E**) Representative images of cell shape. (**F**) Cell size was increased by TGF-β1 treatment, which was ameliorated by miR-30c-1. (**G**) Representative images of yes-associated protein 1 (YAP). (**H**) YAP levels were quantified. (**I**) miR-30c-l levels were reduced in treatment with TGF-β1. *statistically significant.

DISCUSSION

miR-30c-1 promotes the proliferation of hCECs

miR-30c-1 is a component of the miR-30 family and there are six miR-30 genes present in the human genome; [10] the miR-30c-1 gene is positioned at chromosome 1 and the miR-30c-2 gene at chromosome 6 [11], but their roles may differ due to their differing sequences. miR-30c-1 is cut into miR-30c-1-5p and miR-30c-1-3p which then bind to target sites including TGFβR2, [12] p16INK4A, [13] NOV/CCN3, [14] RUNX2, [15] KRAS, [8] SNAI1, [16] SNAI2, TWF1, and VIM [17]. This study revealed that miR-30c-1 promotes cell viability and proliferation in hCECs, which was associated with cell cycle analysis. Proliferation-associated genes such as *CDC25B, CCNG1, CCNG2, CCNA2, CCND2, CDK6, CDKN2A/2B and NOTCH1/2* mRNA expressions were changed in treatment with miR-30c-1. miR-30c-1 has been reported to increase stem cell proliferation. [9, 18, 19] Cyclins drives the cell cycle, [20] and elevated the cyclins levels, which is related with a high proliferation rate [20]. The p16INK4A/CDKN2A protein inhibits

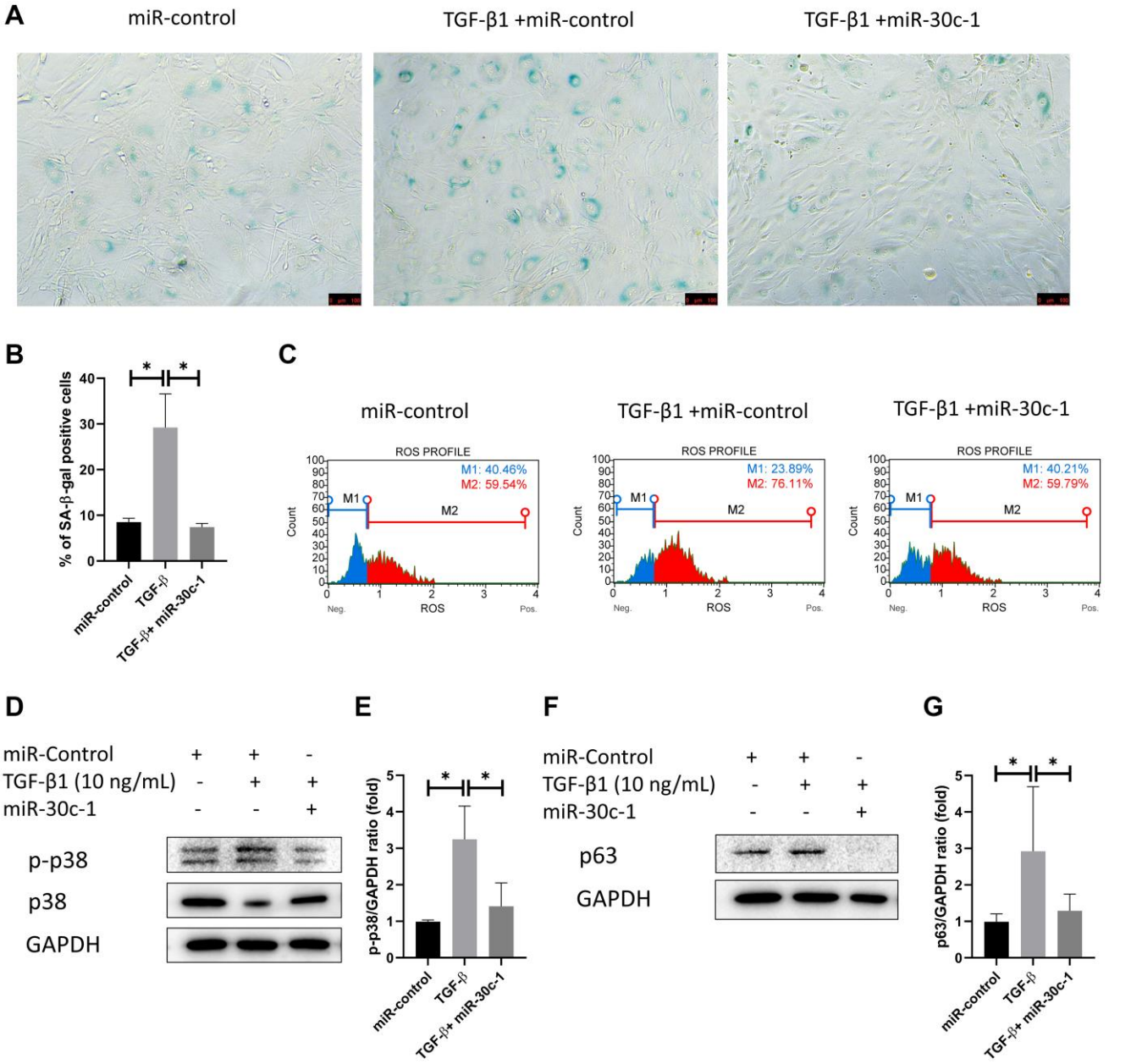

Figure 5. miR-30c-1 ameliorates TGF-β1-induced senescence. (**A**) Representative images of senescence-β-galactosidase (SA-β-gal) staining. (**B**) The percentage of SA-β-gal positive cells was quantified. (**C**) Intracellular oxidative stress levels measured by MitoSOX probe. (**D**) Representative images of p-p38 and p38. (**E**) Activation of p38 was quantified. (**F**) Representative images of p63. (**G**) p63 level was quantified. *statistically significant.

CDK4/6-cyclin D and phosphorylation of the Rb protein, thereby inducing cell cycle cessation in G1-phase. miR-30 inhibits p16INK4A/CDKN2A in murine cancer model [13]. Notch1 mediates local cell-cell communication, inhibits cell proliferation, and causes premature cell cycle exit; [21] notch1 can also inhibit Rb

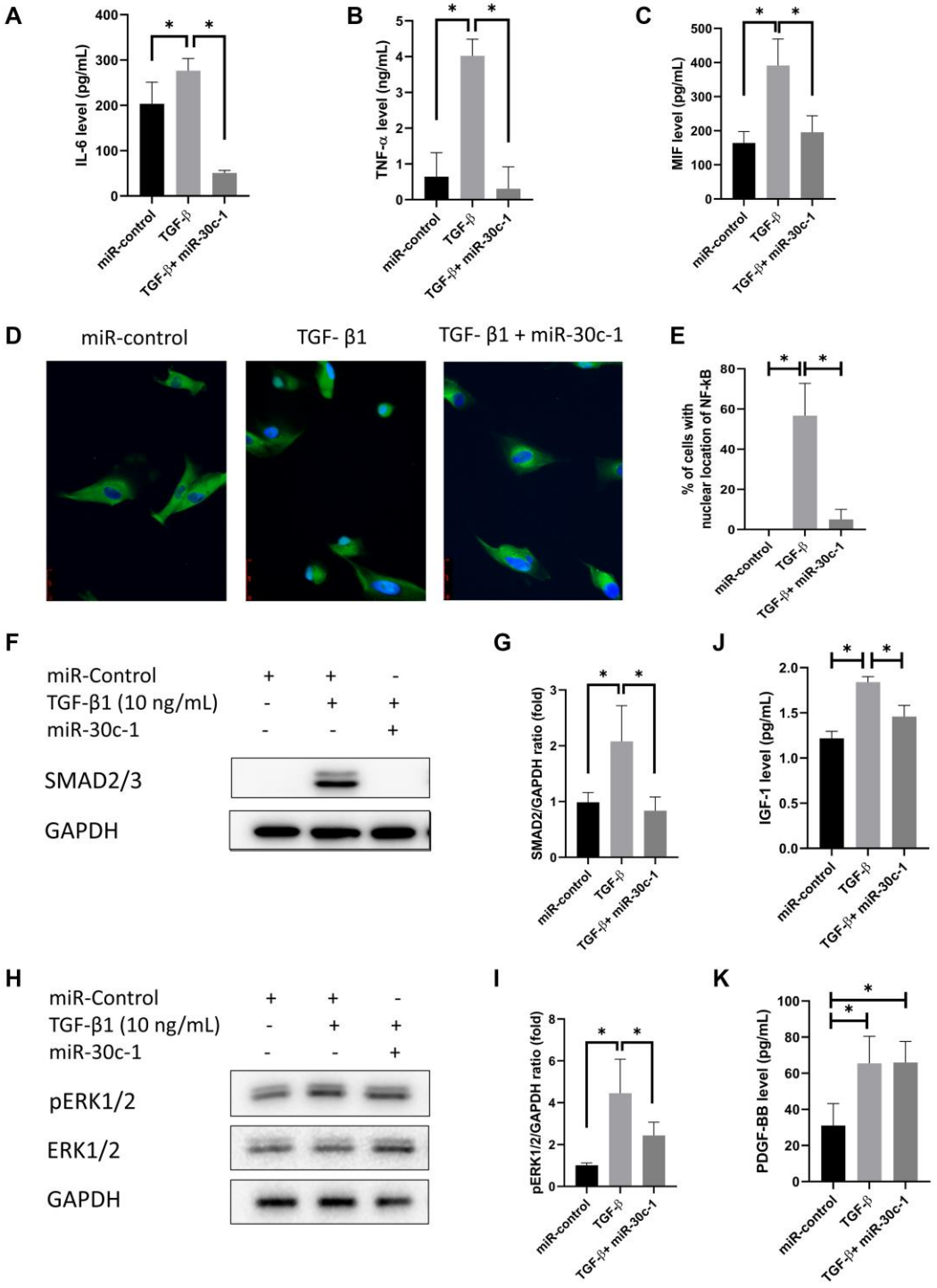

Figure 6. Senescence-associated secretory phenotype (SASP) factors. (**A**–**C**) Interleukin-6 (IL-6; A), tumor necrosis factor-α (TNF-α; B), macrophage migration inhibitory factor (MIF; C) levels were evaluated by ELISA. (**D**) Representative images of immunofluorescence staining of nuclear factor kappa-light-chain-enhancer of activated B cells (NF-κB). (**E**) Nuclear translocation of Nf-κB was evaluated and quantified. Immunofluorescence staining of NF-κB p65 (green) and nuclear with Hoechst 33342 (blue) was performed. (**F**–**G**) SMAD2/3 levels were evaluated by western blotting. (**H**–**I**) pERK1/2 levels were evaluated by western blotting. (**J**) Insulin-like growth factor-1 (IGF-1) levels were evaluated by ELISA. (**K**) Platelet-derived growth factor-BB (PDGF-BB) were evaluated by ELISA. *statistically significant.

phosphorylation in primary endothelial cell and induce cell cycle arrest [22]. miR-30c-1 has been reported to suppress NOTCH signaling [23]. IFN-associated genes and TGF-β-associated genes were decreased with in treatment with miR-30c-1. IFN is a group of signaling proteins that participates in immune reaction against infections and that induces apoptosis [24, 25]. TGF-β regulates various cell functions including fibrosis, senescence and apoptosis [26–28]. miR-30c has been reported to suppress the IFN response by targeting JAK1 and TGF-β response by targeting serpine1 [12, 29, 30]. Caspases and autophagy-associated genes were

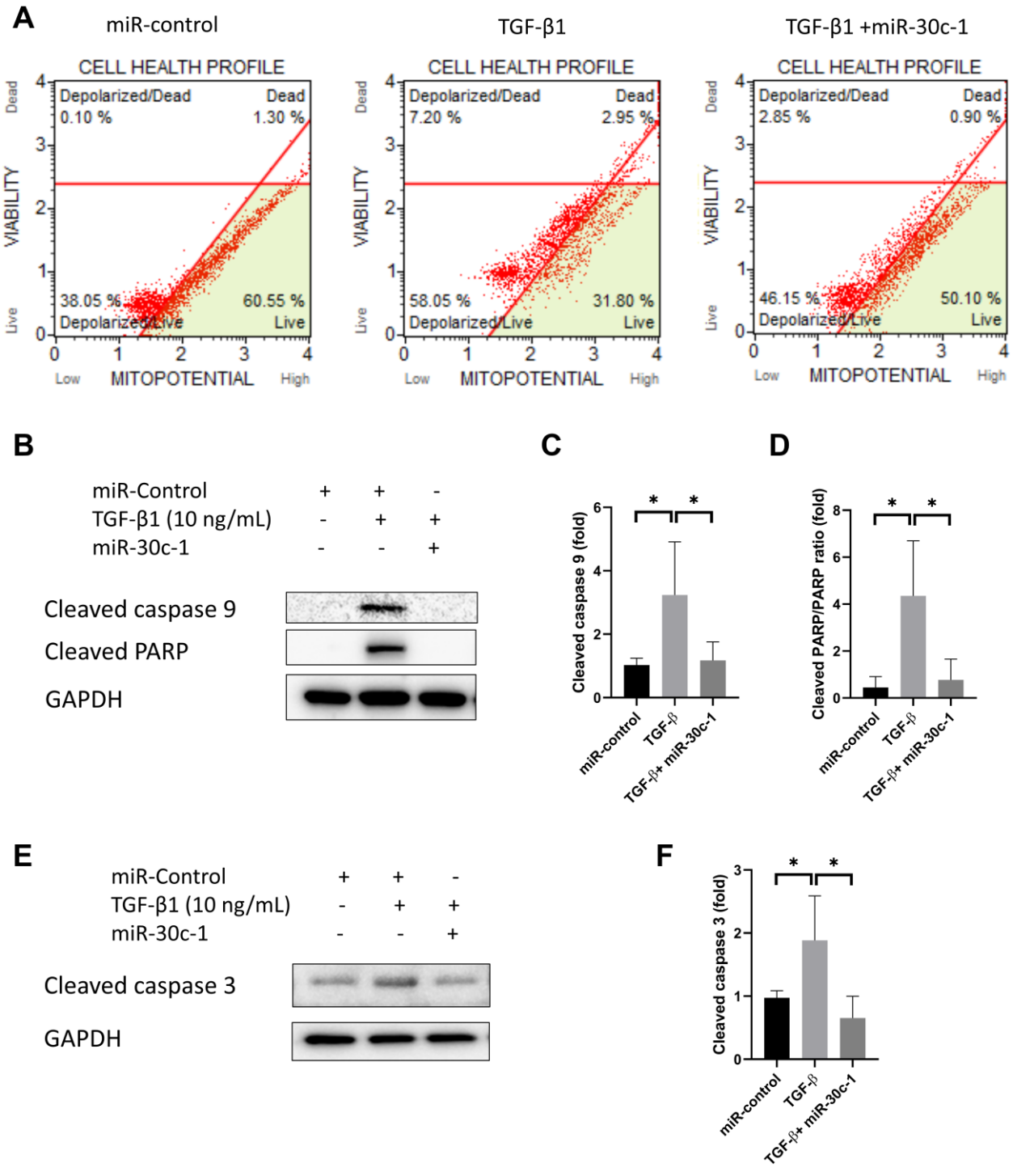

Figure 7. Cell death by TGF-β1 or miR-30c-1. (**A**) Mitochondrial membrane potential was measured by MitoPotential kit. (**B**–**D**) Cleaved caspase 9 and cleaved poly ADP ribose polymerase (PARP) levels were evaluated by western blotting and quantified. (**E**–**F**) Cleaved caspase 3 was evaluated by western blotting and quantified. *statistically significant.

decreased with in treatment with miR-30c-1. Caspases are the executioners of apoptosis that involved in mediating cell death [31]. Autophagy is a recycling and degradative process that delivers cytoplasmic materials to the lysosome [32] and associated with cell death [33].

In the present study, we found that miR-30c-1 reduced intracellular oxidative stress and increased mitochondrial membrane potential. Oxidative stress participates in pathogenesis of FECD or hCEC diseases. Reactive oxygen species (ROS) are produced in mitochondria and excess ROS leads to disruption of cellular function, senescence, inflammation, and apoptosis [34]. miR-30c-5p has been described to suppress oxidative stress-caused cardiomyocyte apoptosis and p53 expression [35]. Mitochondrial membrane potential is a powerful regulator of mitochondrial generation of ROS that performs physiological and pathological functions and is a component of the quality control machinery of mitochondria [20]. miR-30c mimics have been shown to significantly preserve mitochondria membrane potential [36]. In conclusion, miR-30c-1 increased cell viability and proliferation, modulated signaling pathways, and reduced oxidative stress. Thus, miR-30c-1 may be a target for regeneration of hCECs.

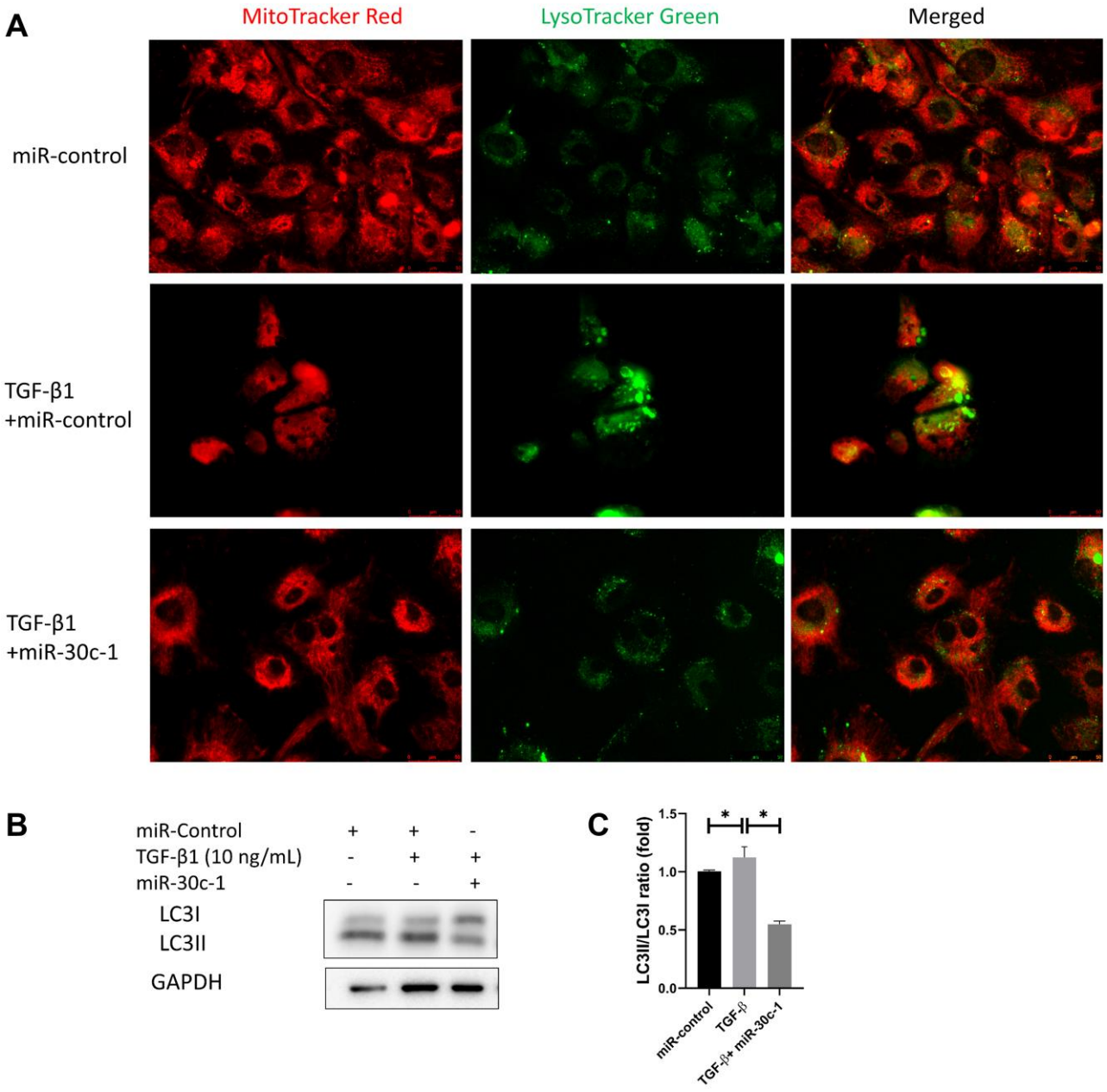

Figure 8. Autophagy by TGF-β1 or miR-30c-1. (**A**) Mitochondria (red) and lysosomes (green) were staining. (**B**) Representative images of microtubule-associated protein 1A/1B-light chain 3 (LC3). (**C**) LC3I and LC3II levels were quantified. *statistically significant.

miR-30c-1 ameliorates TGF-β1-induced senescence of hCECs

This study showed that TGF-β1 induces senescence in hCECs. Senescence is cell cycle cessation and is accompanied by cell shape changes, metabolic reprogramming, and release of the SASP [20]. Staining of SA-β-gal is widely used as a sign for senescence [37]. In this study, the ratio of SA-β-gal-stained cells elevated after TGF-β1 treatment, while other senescence-associated changes including cell enlargement, increase of ROS levels and depolarization of mitochondrial membrane potential occur after TGF-β1 treatment. TGF-β1 inhibited cell proliferation and induced cell hypertrophy, which is similar to the wound healing process with *in vivo* hCECs. TGF-β1 blocks cell cycle progression as it prevents cyclin D production and increases INK4, which inhibits RB phosphorylation through binding to CDK4/6 and causing the redistribution of p27 to CDK2-cyclin E. TGF-β1 also increases intracellular oxidative stress level by inducing NADPH oxidases and suppressing antioxidant systems, which results in redox imbalance [38]. Excess ROS leads to apoptosis through the loss of mitochondrial membrane potential [39], which enhances apoptosis by secretion of apoptogenic factors and decline of energy production [20].

In this study, TGF-β1 induced senescence and increased intracellular oxidative stress levels, which were ameliorated by treatment with miR-30c-1. During senescence, TGF-β1 stimulus increased intracellular oxidative stress level [40], which activates p38 [18] and, subsequently, the p53 growth arrest pathway [18]. Cell cycle arrest is linked to accumulated SA-β-gal, while p63 has been known as a mediator of senescence and aging [41]. DNA damage by ROS activates p63 regulation of AMPK and sirtuin 1 (SIRT1) activity, and induces mitochondria dysfunction. TGFβR2 is a validated target of miR-30c-1-3p [12], which binds to the 3'-UTR of TGFβR2 [12] and disrupts senescence by inhibiting p16INK4A and DNA damage pathways via suppression of CHD7 and TNRC6A [13]. TGF-β1 signaling is inhibited by miR-30c genes [42, 43].

This study showed that miR-30c-1 ameliorated TGF-β1-induced cell cycle cessation and TGF-β1-induced cellular hypertrophy. In cell cycle analysis, TGF-β1 caused G0/G1 cell cycle cessation, which is similar to hCECs *in vivo*. hCECs respond to wound healing by increasing cell size, where the TGF-β signaling pathway may play an important role. miR-30c-1 blocked TGFβR2, [12] which is critical for TGF-β signaling. YAP is a member of hippo signaling pathway, which controls cellular senescence [44]. Hippo-YAP pathway increases organ size through LATS-induced phosphorylation [45].

SASP factors including IL-6, TNF-α, and MIF were increased by TGF-β1 stimulus. SASP factors, which are mostly proinflammatory proteins, are released from senescent cells and activate the immune system and the EMT [46]. NF-κB participates in the modulation of immunological processes that stimulate the production of SASPs [47]. SMAD2 is a component of the TGF-β1 signaling pathway, and after activation by TGF-β1, enters the nucleus and activates the target gene promoting EMT [48]. miR-30c inhibits NF-κB signaling, thus inhibiting the SASP factors. Knockdown of NF-κB activity has been reported to reduce secretion of SASP factors [49].

TGF-β1 significantly stimulated the secretion of IGF-I and PDGF-BB [50–52]. IGF-1 is the inducer for senescence and is linked to organismal aging [53]. Up-regulated IGF-1 signaling maintains p21 level via the Ras-mitogen activated protein (MAP) kinase pathway, which contributes to reduce proliferation, to elevate cellular senescence, and to promote aging phenotypes [53]. IGF signaling is inhibited by miR-30c [42]. PDGF-BB binds to cell membrane tyrosine kinase receptor, promotes wound healing, cell proliferation and EMT [20]. The number of PDGF-BB receptors increases in senescent cell [54], although TGF-β signaling has been described to induce the production of PDGF-B [51].

miR-30c-1 ameliorates TGF-β1-induced cell death of hCECs

This study showed that miR-30c-1 eliminated TGF-β1-induced depolarization of mitochondrial membrane potential. Levels of cleaved caspase-3, cleaved caspase-9, and cleaved PARP were increased by TGF-β1, and this effect was ameliorated by miR-30c-1 treatment. Mitochondrial membrane potential is a reliable measure of cell stress and apoptosis and is decreased during apoptosis [55]. The opening of mitochondrial permeability transition pores causes the loss of the mitochondrial membrane potential, release of cytochrome c, loss of ATP, and increased free radical formation [36, 56]. Caspase 3 is a performer in apoptosis because it coordinates the degradation of cellular structures [57]. Caspase 9 not only cleaves caspases-3, -6, and -7, which are the apoptosis executioners, but also participates in the regulation of autophagy and can facilitate autophagosome formation [58]. PARP is one of several substrates of caspases, and PARP cleavage inhibits the necrosis during apoptosis and guarantees the proper caspase-mediated cell death [59]. miR-30c maintained mitochondria membrane potential and

reduced expression of apoptotic factors. Senescence is resistant to apoptosis induced by genotoxic stress [60]. However, excessive intracellular ROS causes DNA-damage and mitochondrial dysfunction, leading to cell death [61]. Although senescence is resistant to cell death, it is a process leading to cell death [61, 62].

Autophagy is a cellular program characterized by the degrading and recycling protein aggregates and damaged organelles [63]. Autophagy can mediate the transition to a senescent phenotype [64]. Inhibition of miR-30 encourages myocardial hypertrophy via exorbitant autophagy [65]. miR-30 family inhibits the BECN1 expression and autophagy [66]. This study showed that miR-30c-1 treatment eliminated TGF-β1-induced autophagy. TGF-β1 induces autophagy through the SMAD and JNK pathways [67]. The lysosome is a cellular center for signaling, metabolism, and quality control [68], where autophagy acts as a regulated pathway that digests cytoplasmic components and organelles [63]. LC3 is a central molecule in the autophagy pathway [69], and during autophagy, LC3-I (a cytosolic form of LC3) is changed to LC3-II (LC3-phosphatidylethanolamine conjugate), which is an autophagosomal marker [70]. The expression of cytochrome P450 3A4, which participates in the energy metabolism, is altered by miR-30c-1 [11]. miR-30c participates in regulation of autophagy through direct targeting BECN1 [71].

CONCLUSIONS

In conclusion, miR-30c-1 promoted the proliferation of hCECs by ameliorating TGF-β1-induced senescence and reducing cell death of hCECs. Therefore, miR-30c-1 may be a valuable therapeutic target for regeneration of hCECs.

MATERIALS AND METHODS

Cell culture and transfection

This study was reviewed and approved by the institutional review board/ethics committee of Hallym University Kangnam Sacred Heart Hospital and was conducted in accordance with the Helsinki Declaration. Cells were cultured in accordance with previously published methods [72]. The corneas from six donors were used. hCECs were detached from Descemet's membrane by trypsinizing for 10 min. The cells were cultured in 6-well plates applied with a fibronectin–collagen combination (FNC) coating mix (Athena Environmental Sciences, Inc., Baltimore, MD) and passaged at a ratio of 1:3 [72].

hCECs were transfected with human miR-30c-1 (5′-UGUAAACAUCCUACACUCUCAGC-3′; Bioneer corp., Daejeon, Korea) or mimic negative control (SMC-2002, Bioneer corp.; miR-control) using Lipofectamine™ RNAiMAX reagent (Invitrogen, Carlsbad, CA). Cells were treated for 48–72 h and then collected for the experiments. The expression of miR-30c-1 was confirmed by RT-qPCR at 48 h after transfection. In addition, hCECs were treated with and without TGF-β1 (10 ng/mL) and miR-30c-1 or miR-control for 72 h to evaluate the effect of hsa-miR-30c-1 on TGF-β1-treated cells.

Cell viability and proliferation assay

Cells (1×10^4) per well were seeded in a 96-well plate and treated with miRNA for 48–72 h. Cell viability was evaluated using a cell counting kit-8 (CCK-8; Dojindo, Kumamoto) [73]. After incubation with CCK-8 solution for 1–2 h, a Synergy HTX (BioTEK, Winooski, VT) multi-mode reader was used for evaluating cell viability by measuring optical density (OD) at 450 nm [73]. A bromodeoxyuridine (BrdU) incorporation assay kit (Roche Diagnostics, GmbH, Mannheim, Germany) was employed for evaluating cell proliferation rate according to manufacturer's protocol [72].

Cell cycle analysis

Muse cell analyzer (Merck Millipore, Burlington, MA) and propidium iodide (PI) staining was used for evaluating cell cycle analysis [74].

Immunofluorescent staining

Immunofluorescent staining was performed as previously described [75]. Rabbit anti-human nuclear factor kappa-light-chain-enhancer of activated B cells (NF-κB) antibody (sc-372; Santa Cruz Biotechnology, Santa Cruz, CA) was applied as primary antibody and fluorescein isothiocyanate-conjugated goat anti-rabbit IgG antibody was applied as secondary antibody [75]. Nuclear counterstaining was conducted with Hoechst 33342 dye. The pictures were taken using fluorescence microscopy (DMi8; Leica).

Enzyme-linked immunosorbent assay (ELISA)

The conditioned medium was obtained and stored at –70°C until used to evaluate the SASP secretion levels. The levels of interleukin-6 (IL-6), tumor necrosis factor-α (TNF-α), macrophage migration inhibitory factor (MIF), insulin-like growth factor 1 (IGF-1) and platelet-derived growth factor-BB (PDGF-BB) in the conditioned medium were measured using commercial human IL-6, TNF-α, MIF, IGF-1, and PDGF-BB ELISA kits (R&D Systems, Minneapolis, MN) [76]. In brief, capture anti-human IL-6, TNF-α, MIF, IGF-1, and

PDGF-BB antibodies was applied to each well of 96-well plates overnight at 25°C. The wells were incubated with a blocking buffer containing 1% (w/v) BSA at 25°C for 1 h. Standard dilutions, 100 μL, of the commercial prepared human IL-6, TNF-α, MIF, IGF-1, and PDGF-BB, together with the experimental samples were applied to each well. After incubation at 25°C for 2 h, the plates were treated with goat anti-human IL-6, TNF-α, MIF, IGF-1, and PDGF-BB antibody conjugated to horseradish peroxidase (HRP) at 25°C for 2 h. Then, the plates were treated with a color reagent (3,3′,5,5′-tetramethylbenzidine [TMB]) for 20 min to obtain a blue color. Then, 1 M H_2SO_4 stop solution was applied. The OD was evaluated at 450 nm using a Synergy HTX multi-mode reader.

Western blot

Radioimmunoprecipitation assay buffer (Biosesang, Seoul), supplemented with phosphatase (PhosSTOP; Roche, Basel) inhibitor cocktails and protease (Sigma-Aldrich, St. Louis, MO), was employed to obtain total proteins. SDS-PAGE electrophoresis and western blotting was conducted according to standard protocols. In brief, 5% skim milk was applied for inhibiting the nonspecific binding. The primary antibodies were as follows: rabbit anti- extracellular signal-regulated protein kinases 1 and 2 (ERK1/2) antibody (ab17942, Abcam); rabbit anti- phospho-ERK1/2 (pERK1/2) antibody (ab4819, Abcam); mouse anti- SMAD2/3 antibody (sc-133098, Santa Cruz); rabbit anti-p38 antibody (sc-535, Santa Cruz); mouse anti-p-p38 antibody (sc-7973, Santa Cruz); rabbit anti-p63 antibody (ab124762, Abcam); mouse anti-YAP antibody (sc-376830, Santa Cruz); rabbit anti-caspase 3 antibody (sc-7148, Santa Cruz); mouse anti-caspase 9 antibody (sc-56076, Santa Cruz); mouse anti-LC3 antibody (M186-3, MBL); rabbit anti-PARP antibody (sc-9542, Santa Cruz); or rabbit anti-GAPDH antibody (LF-PA0212, Abfrontier). After washing, an HRP-conjugated secondary antibody and a WEST-Queen™ western blot detection kit (iNtRON Biotechnology, Seongnam, Kyounggi-do) were applied for the detection of protein bands. Video image analysis (Luminograph II, Atto, Tokyo) was used to quantify the data [72].

Real time reverse transcription polymerase chain reaction (RT-qPCR)

ReliaPrep™ RNA Miniprep Systems (Promega Cooperation, Madison, WI) was used to extract total RNA. Nanodrop method was used to measure RNA concentrations. GoScript™ Reverse Transcription System (Promega Cooperation) was used to synthesize first-strand cDNA from 0.2 μg of total RNA with oligonucleotide primers. AccuPower® 2X GreenStar™ qPCR Master Mix (Bioneer) with RT-qPCR primer was used to perform RT-qPCR. The thermocycling parameters were as follows: 95°C for 10 minutes, 40 cycles at 95°C for 15 sec and at 60°C for 1 min [72]. SYBR green fluorescence intensity was taken. *β-actin* gene served as a refence gene. Melting curve analysis was employed to identify the purity of amplified products. ΔΔCq method was used to analyze RT-qPCR [72]. The reverse transcription primers were described in Supplementary Table 1.

RNA sequencing analysis

ReliaPrep™ RNA Miniprep Systems (Promega Cooperation) was used for extraction of RNA from the cultured hCECs. RNA concentrations were measured by Nanodrop equipment. RNA sequencing analysis was conducted by Macrogen, lnc. (Seoul, http://www.macrogen.com/) [77]. In this study, gene expression values were obtained through transcriptome sequencing of Homo sapiens. NEBNext® Ultra™ DNA Library Prep Kit for Illumina® (NEB, USA) was used for libraries preparation of RNA samples. The sequencing libraries were prepared by random fragmentation of cDNA sample, which was followed by PCR amplification [77]. Illumina Hiseq 2500 platform was used for sequencing, which was performed by Macrogen, lnc [78, 79]. Fragments per kilobase of transcript per million mapped (TPM) value was employed to interpret individual gene expression level [77].

Senescence-β-galactosidase assay

Senescence-β-galactosidase (SA-β-gal) staining kit (Biovision) was employed. Briefly, after the media was removed from the cells, each well was incubated in fixative solution for 10–15 min at 25°C. The SA-β-gal staining solution was applied at 37°C overnight in a dry incubator.

Intracellular and mitochondrial oxidative stress evaluation

Dichloro-dihydro-fluorescein diacetate (DCFH-DA; Invitrogen, Carlsbad, CA) was employed to evaluate intracellular ROS levels. Cells were plated in cover glass-bottomed dishes and treated with miR-control or miR-30c-1. Cells were incubated with DCF-DA (10 μM) at 37°C for 1 h, washed, and observed under fluorescence microscopy (DMi8; Leica).

MitoSOX™ Red (Invitrogen) was employed to assess mitochondrial superoxide production. The cells were stained with MitoSOX™ reagent (5 μM) for 10 min at 37°C [74]. Muse cell analyzer was used to evaluate fluorescence intensity.

MitoTracker red and lysosome staining

Mitochondrial mass was measured using MitoTracker red FM fluorescent probe (Invitrogen). Cells (1×10^4) were treated with 200 nM MitoTracker red FM fluorescent probe for 30 min. Muse cell analyzer was used for analysis [72]. The cells were seeded in cover glass-bottom dishes, incubated with LysoTracker green (Invitrogen; 50 nM) and MitoTracker red (200 nM) for 30 min. The cells were observed under fluorescence microscopy (DMi8; Leica).

MitoPotential assay

Mitochondrial membrane potential was assessed using Muse™ MitoPotential assay (Merck Millipore) [73]. Muse™ Cell Analyzer was used for analysis.

Statistics

Data were presented as mean ± standard deviation. Experiments were repeated three times, and a representative experiment is shown. To compare two groups, an independent *t*-test was applied. GraphPad Prism 8 was used for statistical analyses.

AUTHOR CONTRIBUTIONS

Jin Sun Hwang and Young Joo Shin performed the experiments. Younghwan Bae and Young Joo Shin analyzed the data. Jin Sun Hwang and Young Joo Shin designed the study. Younghwan Bae, Jin Sun Hwang and Young Joo Shin wrote the draft of the manuscript and revised the manuscript. All authors have read and approved the final submitted manuscript.

CONFLICTS OF INTEREST

The authors declare no conflicts of interest.

FUNDING

This study was supported by the National Research Foundation (NRF) grant (NRF-2018R1A2B6002251) funded by the Korea government and Hallym University Research Fund.

REFERENCES

1. Matsubara M, Tanishima T. Wound-healing of the corneal endothelium in the monkey: a morphometric study. Jpn J Ophthalmol. 1982; 26:264–73. PMID:7154423

2. Fujikawa LS, Wickham MG, Binder PS. Wound healing in cultured corneal endothelial cells. Invest Ophthalmol Vis Sci. 1980; 19:793–801. PMID:7390726

3. Tamori Y, Deng WM. Compensatory cellular hypertrophy: the other strategy for tissue homeostasis. Trends Cell Biol. 2014; 24:230–7. https://doi.org/10.1016/j.tcb.2013.10.005 PMID:24239163

4. Yang HJ, Sato T, Matsubara M, Tanishima T. [Wound healing of the corneal endothelium in the bullous keratopathy after keratoplasty]. Nippon Ganka Gakkai Zasshi. 1983; 87:701–7. PMID:6362369

5. Bartel DP. MicroRNAs: genomics, biogenesis, mechanism, and function. Cell. 2004; 116:281–97. https://doi.org/10.1016/s0092-8674(04)00045-5 PMID:14744438

6. Lee JY, Park EH, Lee S, Ko G, Honda Y, Hashizume M, Deng F, Yi SM, Kim H. Airborne Bacterial Communities in Three East Asian Cities of China, South Korea, and Japan. Sci Rep. 2017; 7:5545. https://doi.org/10.1038/s41598-017-05862-4 PMID:28717138

7. Matthaei M, Hu J, Kallay L, Eberhart CG, Cursiefen C, Qian J, Lackner EM, Jun AS. Endothelial cell microRNA expression in human late-onset Fuchs' dystrophy. Invest Ophthalmol Vis Sci. 2014; 55:216–225. https://doi.org/10.1167/iovs.13-12689 PMID:24334445

8. Shi L, Middleton J, Jeon YJ, Magee P, Veneziano D, Lagana A, Leong HS, Sahoo S, Fassan M, Booton R, Shah R, Crosbie PAJ, Garofalo M. KRAS induces lung tumorigenesis through microRNAs modulation. Cell Death Dis. 2018; 9:219. https://doi.org/10.1038/s41419-017-0243-9 PMID:29440633

9. Liu X, Li M, Peng Y, Hu X, Xu J, Zhu S, Yu Z, Han S. miR-30c regulates proliferation, apoptosis and differentiation via the Shh signaling pathway in P19 cells. Exp Mol Med. 2016; 48:e248. https://doi.org/10.1038/emm.2016.57 PMID:27469029

10. Bridge G, Monteiro R, Henderson S, Emuss V, Lagos D, Georgopoulou D, Patient R, Boshoff C. The microRNA-30 family targets DLL4 to modulate endothelial cell behavior during angiogenesis. Blood. 2012; 120:5063–72. https://doi.org/10.1182/blood-2012-04-423004 PMID:23086751

11. Vachirayonstien T, Yan B. MicroRNA-30c-1-3p is a silencer of the pregnane X receptor by targeting the 3'-untranslated region and alters the expression of its target gene cytochrome P450 3A4. Biochim Biophys

Acta. 2016; 1859:1238–1244.
https://doi.org/10.1016/j.bbagrm.2016.03.016
PMID:27085140

12. Wu M, Liang G, Duan H, Yang X, Qin G, Sang N. Synergistic effects of sulfur dioxide and polycyclic aromatic hydrocarbons on pulmonary pro-fibrosis via mir-30c-1-3p/ transforming growth factor beta type II receptor axis. Chemosphere. 2019; 219:268–276.
https://doi.org/10.1016/j.chemosphere.2018.12.016
PMID:30543962

13. Su W, Hong L, Xu X, Huang S, Herpai D, Li L, Xu Y, Truong L, Hu WY, Wu X, Xiao C, Zhang W, Han J, et al. miR-30 disrupts senescence and promotes cancer by targeting both p16(INK4A) and DNA damage pathways. Oncogene. 2018; 37:5618–5632.
https://doi.org/10.1038/s41388-018-0358-1
PMID:29907771

14. Dobson JR, Taipaleenmaki H, Hu YJ, Hong D, van Wijnen AJ, Stein JL, Stein GS, Lian JB, Pratap J. hsa-mir-30c promotes the invasive phenotype of metastatic breast cancer cells by targeting NOV/CCN3. Cancer Cell Int. 2014; 14:73.
https://doi.org/10.1186/s12935-014-0073-0
PMID:25120384

15. Zhang Y, Xie RL, Croce CM, Stein JL, Lian JB, van Wijnen AJ, Stein GS. A program of microRNAs controls osteogenic lineage progression by targeting transcription factor Runx2. Proc Natl Acad Sci U S A. 2011; 108:9863–8.
https://doi.org/10.1073/pnas.1018493108
PMID:21628588

16. Zhang J, Zhang H, Liu J, Tu X, Zang Y, Zhu J, Chen J, Dong L, Zhang J. miR-30 inhibits TGF-beta1-induced epithelial-to-mesenchymal transition in hepatocyte by targeting Snail1. Biochem Biophys Res Commun. 2012; 417:1100–5.
https://doi.org/10.1016/j.bbrc.2011.12.121
PMID:22227196

17. Bockhorn J, Yee K, Chang YF, Prat A, Huo D, Nwachukwu C, Dalton R, Huang S, Swanson KE, Perou CM, Olopade OI, Clarke MF, Greene GL, et al. MicroRNA-30c targets cytoskeleton genes involved in breast cancer cell invasion. Breast Cancer Res Treat. 2013; 137:373–382.
https://doi.org/10.1007/s10549-012-2346-4
PMID:23224145

18. Freund A, Patil CK, Campisi J. p38MAPK is a novel DNA damage response-independent regulator of the senescence-associated secretory phenotype. EMBO J. 2011; 30:1536–48.
https://doi.org/10.1038/emboj.2011.69
PMID:21399611

19. Zou YF, Liao WT, Fu ZJ, Zhao Q, Chen YX, Zhang W. MicroRNA-30c-5p ameliorates hypoxia-reoxygenation-induced tubular epithelial cell injury via HIF1alpha stabilization by targeting SOCS3. Oncotarget. 2017; 8:92801–92814.
https://doi.org/10.18632/oncotarget.21582
PMID:29190957

20. Ahlin C, Lundgren C, Embretsen-Varro E, Jirstrom K, Blomqvist C, Fjallskog M. High expression of cyclin D1 is associated to high proliferation rate and increased risk of mortality in women with ER-positive but not in ER-negative breast cancers. Breast Cancer Res Treat. 2017; 164:667–678.
https://doi.org/10.1007/s10549-017-4294-5
PMID:28528450

21. Andersson ER, Sandberg R, Lendahl U. Notch signaling: simplicity in design, versatility in function. Development. 2011; 138:3593–612.
https://doi.org/10.1242/dev.063610
PMID:21828089

22. Noseda M, Chang L, McLean G, Grim JE, Clurman BE, Smith LL, Karsan A. Notch activation induces endothelial cell cycle arrest and participates in contact inhibition: role of p21Cip1 repression. Mol Cell Biol. 2004; 24:8813–22.
https://doi.org/10.1128/mcb.24.20.8813-8822.2004
PMID:15456857

23. Miranda K, Yang X, Bam M, Murphy EA, Nagarkatti PS, Nagarkatti M. MicroRNA-30 modulates metabolic inflammation by regulating Notch signaling in adipose tissue macrophages. Int J Obes (Lond). 2018; 42:1140–1150.
https://doi.org/10.1038/s41366-018-0114-1
PMID:29899524

24. Chawla-Sarkar M, Lindner DJ, Liu YF, Williams BR, Sen GC, Silverman RH, Borden EC. Apoptosis and interferons: role of interferon-stimulated genes as mediators of apoptosis. Apoptosis. 2003; 8:237–49.
https://doi.org/10.1023/a:1023668705040
PMID:12766484

25. Kotredes KP, Gamero AM. Interferons as inducers of apoptosis in malignant cells. J Interferon Cytokine Res. 2013; 33:162–70.
https://doi.org/10.1089/jir.2012.0110
PMID:23570382

26. Ramesh S, Wildey GM, Howe PH. Transforming growth factor beta (TGFbeta)-induced apoptosis: the rise & fall of Bim. Cell Cycle. 2009; 8:11–7.
https://doi.org/10.4161/cc.8.1.7291
PMID:19106608

27. Schuster N, Krieglstein K. Mechanisms of TGF-beta-mediated apoptosis. Cell Tissue Res. 2002; 307:1–14.

https://doi.org/10.1007/s00441-001-0479-6
PMID:11810309

28. Tominaga K, Suzuki HI. TGF-beta Signaling in Cellular Senescence and Aging-Related Pathology. Int J Mol Sci. 2019; 20:5002.
https://doi.org/10.3390/ijms20205002
PMID:31658594

29. Hwang CY, Han YH, Lee SM, Cho SM, Yu DY, Kwon KS. Sestrin2 Attenuates Cellular Senescence by Inhibiting NADPH Oxidase 4 Expression. Ann Geriatr Med Res. 2020; 24:297–304.
https://doi.org/10.4235/agmr.20.0051
PMID:33227845

30. Zhang Q, Huang C, Yang Q, Gao L, Liu HC, Tang J, Feng WH. MicroRNA-30c Modulates Type I IFN Responses To Facilitate Porcine Reproductive and Respiratory Syndrome Virus Infection by Targeting JAK1. J Immunol. 2016; 196:2272–82.
https://doi.org/10.4049/jimmunol.1502006
PMID:26826240

31. Li J, Yuan J. Caspases in apoptosis and beyond. Oncogene. 2008; 27:6194–206.
https://doi.org/10.1038/onc.2008.297
PMID:18931687

32. Denton D, Kumar S. Autophagy-dependent cell death. Cell Death Differ. 2019; 26:605–616.
https://doi.org/10.1038/s41418-018-0252-y
PMID:30568239

33. Doherty J, Baehrecke EH. Life, death and autophagy. Nat Cell Biol. 2018; 20:1110–1117.
https://doi.org/10.1038/s41556-018-0201-5
PMID:30224761

34. Nita M, Grzybowski A. The Role of the Reactive Oxygen Species and Oxidative Stress in the Pathomechanism of the Age-Related Ocular Diseases and Other Pathologies of the Anterior and Posterior Eye Segments in Adults. Oxid Med Cell Longev. 2016; 2016:3164734.
https://doi.org/10.1155/2016/3164734
PMID:26881021

35. Wang L, Chen X, Wang Y, Zhao L, Zhao X, Wang Y. MiR-30c-5p mediates the effects of panax notoginseng saponins in myocardial ischemia reperfusion injury by inhibiting oxidative stress-induced cell damage. Biomed Pharmacother. 2020; 125:109963.
https://doi.org/10.1016/j.biopha.2020.109963
PMID:32036220

36. Yin Z, Zhao Y, He M, Li H, Fan J, Nie X, Yan M, Chen C, Wang DW. MiR-30c/PGC-1beta protects against diabetic cardiomyopathy via PPARalpha. Cardiovasc Diabetol. 2019; 18:7.
https://doi.org/10.1186/s12933-019-0811-7
PMID:30635067

37. Lee BY, Han JA, Im JS, Morrone A, Johung K, Goodwin EC, Kleijer WJ, DiMaio D, Hwang ES. Senescence-associated beta-galactosidase is lysosomal beta-galactosidase. Aging Cell. 2006; 5:187–95.
https://doi.org/10.1111/j.1474-9726.2006.00199.x
PMID:16626397

38. Liu RM, Desai LP. Reciprocal regulation of TGF-beta and reactive oxygen species: A perverse cycle for fibrosis. Redox Biol. 2015; 6:565–577.
https://doi.org/10.1016/j.redox.2015.09.009
PMID:26496488

39. Marchi S, Giorgi C, Suski JM, Agnoletto C, Bononi A, Bonora M, De Marchi E, Missiroli S, Patergnani S, Poletti F, Rimessi A, Duszynski J, Wieckowski MR, et al. Mitochondria-ros crosstalk in the control of cell death and aging. J Signal Transduct. 2012; 2012:329635.
https://doi.org/10.1155/2012/329635
PMID:22175013

40. Lawless C, Jurk D, Gillespie CS, Shanley D, Saretzki G, von Zglinicki T, Passos JF. A stochastic step model of replicative senescence explains ROS production rate in ageing cell populations. PLoS One. 2012; 7:e32117.
https://doi.org/10.1371/journal.pone.0032117
PMID:22359661

41. Orioli D, Dellambra E. Epigenetic Regulation of Skin Cells in Natural Aging and Premature Aging Diseases. Cells. 2018; 7:268.
https://doi.org/10.3390/cells7120268
PMID:30545089

42. Zhang Y, Xie RL, Gordon J, LeBlanc K, Stein JL, Lian JB, van Wijnen AJ, Stein GS. Control of mesenchymal lineage progression by microRNAs targeting skeletal gene regulators Trps1 and Runx2. J Biol Chem. 2012; 287:21926–35.
https://doi.org/10.1074/jbc.m112.340398
PMID:22544738

43. McCann JV, Xiao L, Kim DJ, Khan OF, Kowalski PS, Anderson DG, Pecot CV, Azam SH, Parker JS, Tsai YS, Wolberg AS, Turner SD, Tatsumi K, et al. Endothelial miR-30c suppresses tumor growth via inhibition of TGF-beta-induced Serpine1. J Clin Invest. 2019; 129:1654–1670.
https://doi.org/10.1172/jci123106
PMID:30855280

44. Xie Q, Chen J, Feng H, Peng S, Adams U, Bai Y, Huang L, Li J, Huang J, Meng S, Yuan Z. YAP/TEAD-mediated transcription controls cellular senescence. Cancer Res. 2013; 73:3615–24.

https://doi.org/10.1158/0008-5472.can-12-3793
PMID:23576552

45. Yu FX, Zhao B, Guan KL. Hippo Pathway in Organ Size Control, Tissue Homeostasis, and Cancer. Cell. 2015; 163:811–28. https://doi.org/10.1016/j.cell.2015.10.044 PMID:26544935

46. Coppe JP, Desprez PY, Krtolica A, Campisi J. The senescence-associated secretory phenotype: the dark side of tumor suppression. Annu Rev Pathol. 2010; 5:99–118. https://doi.org/10.1146/annurev-pathol-121808-102144 PMID:20078217

47. Salminen A, Kauppinen A, Kaarniranta K. Emerging role of NF-kappaB signaling in the induction of senescence-associated secretory phenotype (SASP). Cell Signal. 2012; 24:835–45. https://doi.org/10.1016/j.cellsig.2011.12.006 PMID:22182507

48. Xu J, Lamouille S, Derynck R. TGF-beta-induced epithelial to mesenchymal transition. Cell Res. 2009; 19:156–72. https://doi.org/10.1038/cr.2009.5 PMID:19153598

49. Shukla K, Sharma AK, Ward A, Will R, Hielscher T, Balwierz A, Breunig C, Munstermann E, Konig R, Keklikoglou I, Wiemann S. MicroRNA-30c-2-3p negatively regulates NF-kappaB signaling and cell cycle progression through downregulation of TRADD and CCNE1 in breast cancer. Mol Oncol. 2015; 9:1106–19. https://doi.org/10.1016/j.molonc.2015.01.008 PMID:25732226

50. Voci A, Arvigo M, Massajoli M, Garrone S, Bottazzi C, Demori I, Gallo G. IGF-I production by adult rat hepatocytes is stimulated by transforming growth factor-alpha and transforming growth factor-beta1. Eur J Endocrinol. 1999; 140:577–82. https://doi.org/10.1530/eje.0.1400577 PMID:10366413

51. Yuan Y, Yang M, Wang K, Sun J, Song L, Diao X, Jiang Z, Cheng G, Wang X. Excessive activation of the TLR9/TGF-beta1/PDGF-B pathway in the peripheral blood of patients with systemic lupus erythematosus. Arthritis Res Ther. 2017; 19:70. https://doi.org/10.1186/s13075-017-1238-8 PMID:28356164

52. Chow EK, O'Connell RM, Schilling S, Wang XF, Fu XY, Cheng G. TLR agonists regulate PDGF-B production and cell proliferation through TGF-beta/type I IFN crosstalk. EMBO J. 2005; 24:4071–81. https://doi.org/10.1038/sj.emboj.7600867 PMID:16308570

53. Maier B, Gluba W, Bernier B, Turner T, Mohammad K, Guise T, Sutherland A, Thorner M, Scrable H. Modulation of mammalian life span by the short isoform of p53. Genes Dev. 2004; 18:306–319. https://doi.org/10.1101/gad.1162404 PMID:14871929

54. Bae YU, Choi JH, Nagy A, Sung HK, Kim JR. Antisenescence effect of mouse embryonic stem cell conditioned medium through a PDGF/FGF pathway. FASEB J. 2016; 30:1276–86. https://doi.org/10.1096/fj.15-278846 PMID:26675707

55. Zorova LD, Popkov VA, Plotnikov EY, Silachev DN, Pevzner IB, Jankauskas SS, Babenko VA, Zorov SD, Balakireva AV, Juhaszova M, Sollott SJ, Zorov DB. Mitochondrial membrane potential. Anal Biochem. 2018; 552:50–59. https://doi.org/10.1016/j.ab.2017.07.009 PMID:28711444

56. Zaino RJ, Feil PD, Clarke CL, Mortel R, Satyaswaroop PG. A polyclonal antiserum against the rabbit progesterone receptor recognizes the human receptor: immunohistochemical localization in rabbit and human uterus. Cell Biochem Funct. 1989; 7:147–52. https://doi.org/10.1002/cbf.290070211 PMID:2766472

57. McIlwain DR, Berger T, Mak TW. Caspase functions in cell death and disease. Cold Spring Harb Perspect Biol. 2013; 5:a008656. https://doi.org/10.1101/cshperspect.a008656 PMID:23545416

58. Nowikovsky K, Bergmann M. Autophagy regulates apoptosis on the level of the death-inducing signalling complex. FEBS J. 2017; 284:1967–1969. https://doi.org/10.1111/febs.14119 PMID:28670876

59. Germain M, Affar EB, D'Amours D, Dixit VM, Salvesen GS, Poirier GG. Cleavage of automodified poly(ADP-ribose) polymerase during apoptosis. Evidence for involvement of caspase-7. J Biol Chem. 1999; 274:28379–84. https://doi.org/10.1074/jbc.274.40.28379 PMID:10497198

60. Rochette PJ, Brash DE. Progressive apoptosis resistance prior to senescence and control by the anti-apoptotic protein BCL-xL. Mech Ageing Dev. 2008; 129:207–14. https://doi.org/10.1016/j.mad.2007.12.007 PMID:18262222

61. Surova O, Zhivotovsky B. Various modes of cell death induced by DNA damage. Oncogene. 2013;

32:3789–97.
https://doi.org/10.1038/onc.2012.556
PMID:23208502

62. Childs BG, Baker DJ, Kirkland JL, Campisi J, van Deursen JM. Senescence and apoptosis: dueling or complementary cell fates? EMBO Rep. 2014; 15:1139–53.
https://doi.org/10.15252/embr.201439245
PMID:25312810

63. Eskelinen EL, Saftig P. Autophagy: a lysosomal degradation pathway with a central role in health and disease. Biochim Biophys Acta. 2009; 1793:664–73.
https://doi.org/10.1016/j.bbamcr.2008.07.014
PMID:18706940

64. Slobodnyuk K, Radic N, Ivanova S, Llado A, Trempolec N, Zorzano A, Nebreda AR. Autophagy-induced senescence is regulated by p38alpha signaling. Cell Death Dis. 2019; 10:376.
https://doi.org/10.1038/s41419-019-1607-0
PMID:31092814

65. Pan W, Zhong Y, Cheng C, Liu B, Wang L, Li A, Xiong L, Liu S. MiR-30-regulated autophagy mediates angiotensin II-induced myocardial hypertrophy. PLoS One. 2013; 8:e53950.
https://doi.org/10.1371/journal.pone.0053950
PMID:23326547

66. Mao L, Liu S, Hu L, Jia L, Wang H, Guo M, Chen C, Liu Y, Xu L. miR-30 Family: A Promising Regulator in Development and Disease. Biomed Res Int. 2018; 2018:9623412.
https://doi.org/10.1155/2018/9623412
PMID:30003109

67. Suzuki HI, Kiyono K, Miyazono K. Regulation of autophagy by transforming growth factor-beta (TGF-beta) signaling. Autophagy. 2010; 6:645–7.
https://doi.org/10.4161/auto.6.5.12046
PMID:20458184

68. Lawrence RE, Zoncu R. The lysosome as a cellular centre for signalling, metabolism and quality control. Nat Cell Biol. 2019; 21:133–142.
https://doi.org/10.1038/s41556-018-0244-7
PMID:30602725

69. Lee YK, Lee JA. Role of the mammalian ATG8/LC3 family in autophagy: differential and compensatory roles in the spatiotemporal regulation of autophagy. BMB Rep. 2016; 49:424–30.
https://doi.org/10.5483/bmbrep.2016.49.8.081
PMID:27418283

70. Tanida I, Ueno T, Kominami E. LC3 and Autophagy. Methods Mol Biol. 2008; 445:77–88.
https://doi.org/10.1007/978-1-59745-157-4_4
PMID:18425443

71. Chen C, Yang S, Li H, Yin Z, Fan J, Zhao Y, Gong W, Yan M, Wang DW. Mir30c Is Involved in Diabetic Cardiomyopathy through Regulation of Cardiac Autophagy via BECN1. Mol Ther Nucleic Acids. 2017; 7:127–139.
https://doi.org/10.1016/j.omtn.2017.03.005
PMID:28624189

72. Hwang JS, Ma DJ, Choi J, Shin YJ. COL8A2 Regulates the Fate of Corneal Endothelial Cells. Invest Ophthalmol Vis Sci. 2020; 61:26.
https://doi.org/10.1167/iovs.61.11.26
PMID:32931574

73. Hwang JS, Yi HC, Shin YJ. Effect of SOX2 Repression on Corneal Endothelial Cells. Int J Mol Sci. 2020; 21:4397.
https://doi.org/10.3390/ijms21124397
PMID:32575737

74. Joo HJ, Ma DJ, Hwang JS, Shin YJ. SIRT1 Activation Using CRISPR/dCas9 Promotes Regeneration of Human Corneal Endothelial Cells through Inhibiting Senescence. Antioxidants (Basel). 2020; 9:1085.
https://doi.org/10.3390/antiox9111085
PMID:33158256

75. Choi WS, Koh JW, Chung TY, Hyon JY, Wee WR, Shin YJ. Cytotoxicity of ganciclovir on cultured human corneal endothelial cells. Antivir Ther. 2013; 18:813–20.
https://doi.org/10.3851/imp2556
PMID:23462232

76. Shin YJ, Hyon JY, Kim S, Koh JW, Kwon SI, Wee WR. Cysteamine suppresses human peripheral blood mononuclear cells--human corneal endothelial cell reaction via reactive oxygen species reduction. Mol Vis. 2011; 17:3371–78.
PMID:22219632

77. Wang Z, Zhang JW, Zhang Y, Zhang SP, Hu QY, Liang H. Analyses of long non-coding RNA and mRNA profiling using RNA sequencing in calcium oxalate monohydrate-stimulated renal tubular epithelial cells. Urolithiasis. 2019; 47:225–234.
https://doi.org/10.1007/s00240-018-1065-7
PMID:29947995

78. Maina S, Edwards OR, Barbetti MJ, de Almeida L, Ximenes A, Jones RA. Deep Sequencing Reveals the Complete Genome Sequence of Sweet potato virus G from East Timor. Genome Announc. 2016; 4:e00957–16.
https://doi.org/10.1128/genomea.00957-16
PMID:27609925

79. Ju YS, Lee WC, Shin JY, Lee S, Bleazard T, Won JK, Kim YT, Kim JI, Kang JH, Seo JS. A transforming KIF5B and RET gene fusion in lung adenocarcinoma revealed from whole-genome and transcriptome sequencing. Genome Res. 2012; 22:436–45.

https://doi.org/10.1101/gr.133645.111
PMID:22194472

SUPPLEMENTARY MATERIALS

miR-30c-1 inhibitor induces the senescence of hCECs

The number of SA-β-gal positive cells increased in treated with miR-30c-1-3p inhibitor or miR-30c-1-5p inhibitor ($p < 0.001$ for all; Supplementary Figure 1A–1B). Intracellular oxidative stress levels were elevated in treated with miR-30c-1-3p inhibitor or miR-30c-1-5p inhibitor ($p < 0.001$ for all; Supplementary Figure 1C–1D). Cell viability decreased in treated with miR-30c-1-3p inhibitor or miR-30c-1-5p inhibitor ($p = 0.004$ and <0.001; Supplementary Figure 1E). BrdU proliferation rate decreased in treated with miR-30c-1-3p inhibitor or miR-30c-1-5p inhibitor ($p = 0.001$ and <0.001; Supplementary Figure 1F)

TGF-β1 induces the senescence of hCECs

BrdU proliferation rate decreased at 24 h, 48 h, and 72 h compared with 0 h after TGF-β1 treatment ($p = 0.026$, $p = 0.047$, and $p = 0.023$, respectively; Supplementary Figure 2A). Representative images of cell cycle analysis are shown in Supplementary Figure 2B. Cell cycle analysis showed that the number of cells in G0/G1 phase increased at 48 h and 72 h compared with 0 h ($p < 0.001$ for both; Supplementary Figure 2C), while the number of cells in S phase decreased at 48 h and 72 h compared with 0 h ($p = 0.005$ and $p = 0.003$, respectively; Supplementary Figure 2D), and the number of cells in G2/M phase decreased at 48 h and 72 h compared with 0 h ($p = 0.006$ and $p = 0.010$, respectively; Supplementary Figure 2E). The number of SA-β-gal positive cells increased at 24 h, 48 h, and 72 h compared with 0 h after TGF-β1 treatment ($p < 0.001$, $p < 0.001$, and $p < 0.001$, respectively; Supplementary Figure 2F–2G). Cell size increased at 48 h and 72 h compared with 0 h ($p = 0.005$ and $p < 0.001$, respectively; Supplementary Figure 2H–2I).

Intracellular oxidative stress levels were elevated by TGF-β1 at 48 h and 72 h compared with 0 h ($p = 0.034$ and $p = 0.001$, respectively; Supplementary Figure 3A–3B). The pERK1/2 level increased over time after TGF-β1 treatment (Supplementary Figure 3C). The percentage of cells with depolarized mitochondrial membrane potential was elevated at 48 h and 72 h compared with 0 h ($p = 0.002$ and $p = 0.001$, respectively; Supplementary Figure 3D–3E).

Supplementary Figures

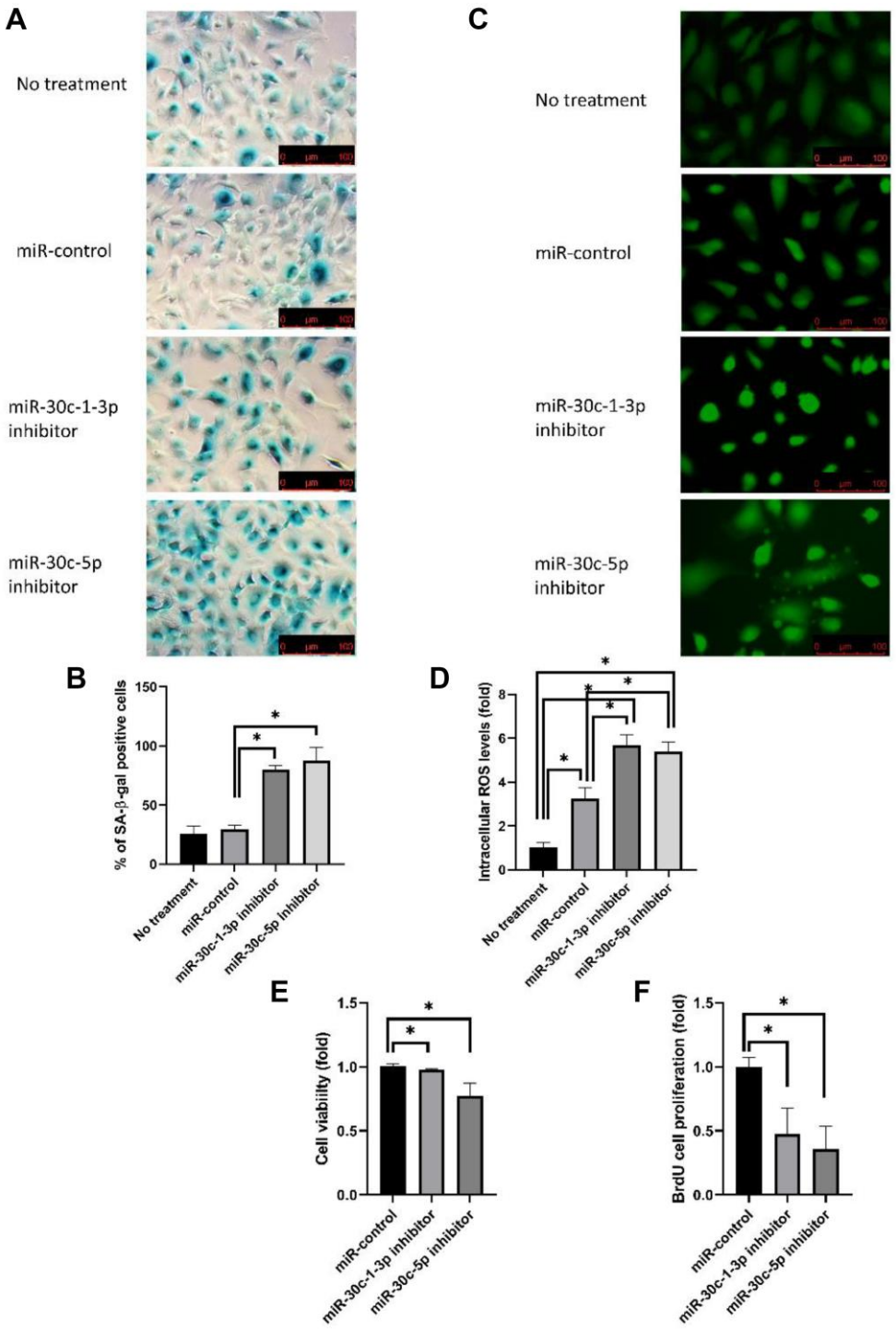

Supplementary Figure 1. miR-30c-1 inhibitor induces the senescence of hCECs. (**A**–**B**) Senescence-associated β-galactosidase positive cells were less shown in treatment with miR-30c-1 inhibitors. (**C**–**D**) Intracellular oxidative stress levels were increased in treatment with miR-30c-1 inhibitors. (**E**–**F**) Cell viability and BrdU cell proliferation rate were decreased in treatment with miR-30c-1 inhibitors. *statistically significant.

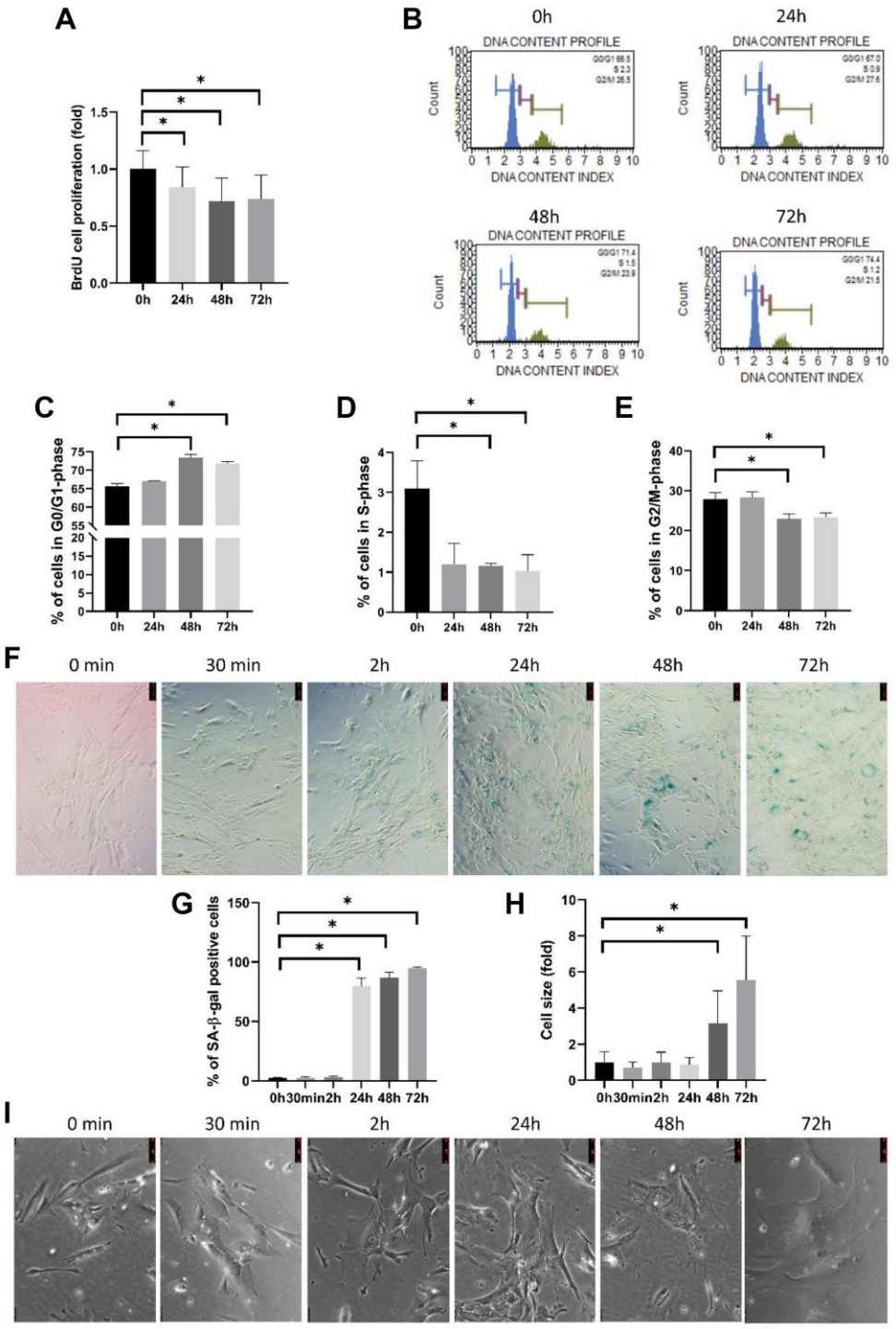

Supplementary Figure 2. Effect of TGF-β1 on cell cycle arrest and senescence. (**A**) Cell proliferation was measured using BrdU proliferation assay. (**B**) Cell cycle analysis using by DNA content measurement. (**C**–**E**) The percentages of cells in G0/G1-phase (C), in S-phase (D) and G2/M-phase (E) were analyzed. (**F**) Representative images of senescence-β-galactosidase (SA-β-gal) staining. (**G**) The percentage of SA-β-gal positive cells was quantified. (**H**) Representative images of cell shape. (**I**) Cell size increased over time after TGF-β1 treatment. *statistically significant.

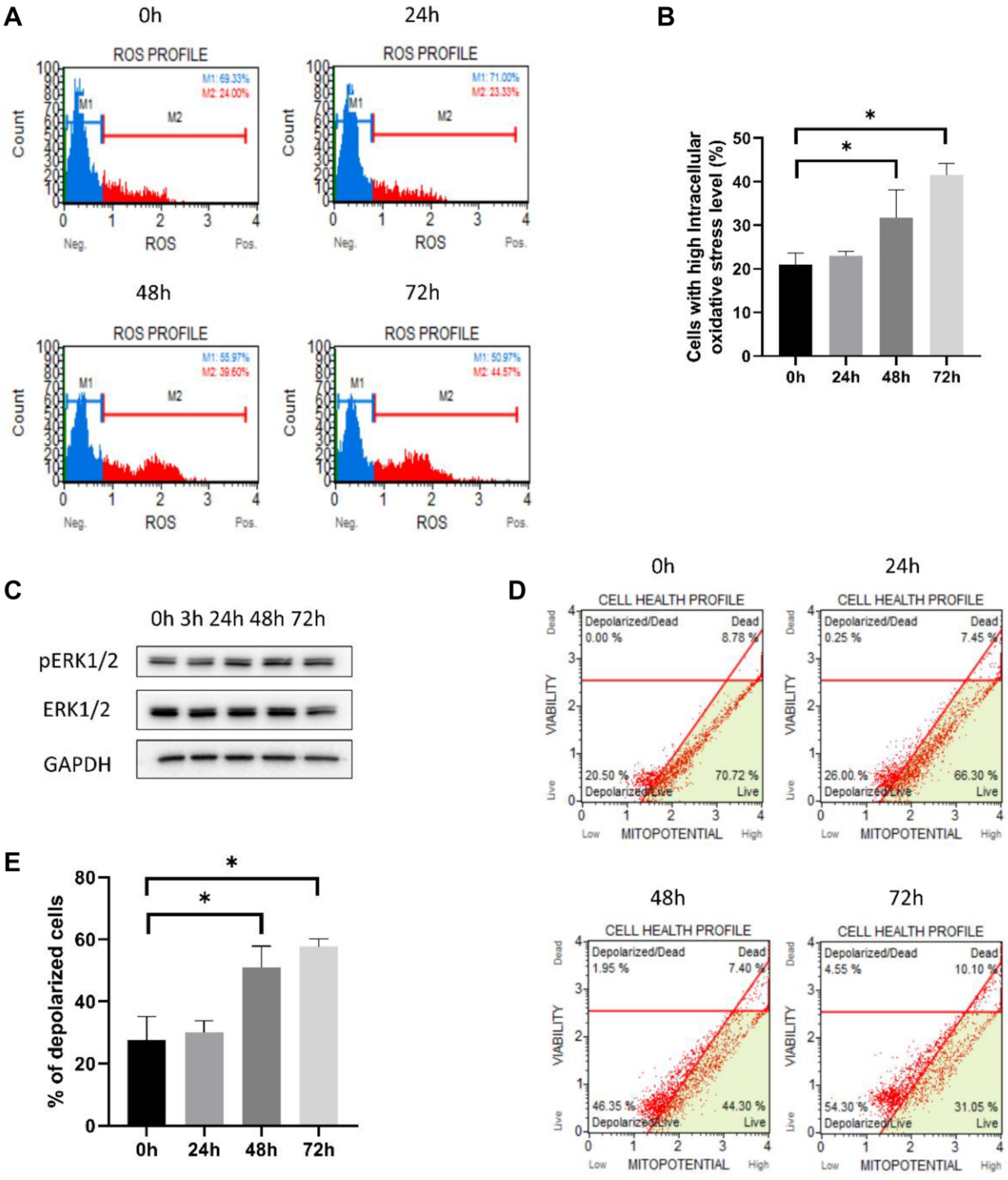

Supplementary Figure 3. Effect of TGF-β1 on mitochondria after TGF-β1 treatment. (**A**) Representative images of oxidative stress levels. (**B**) The percentage of cells with high intracellular oxidative stress level increased over time. (**C**) Activation of ERK increased over time. (**D**) Representative images of mitochondrial membrane potential. (**E**) The percentage of depolarized cells increased over time. *statistically significant.

Supplementary Table

Supplementary Table 1. Primers for RT-qPCR

Gene	Forward primer sequence	Reverse primer sequence
miR-30c-1	TGTGTAAACATCCTACACTCTCAG	GAGTAAACAACCCTCTCCCA